JOURNAL OF MATERIALS SCIENCE 28 (1993) 4553–4561

Electron microscope observations of impact crater debris amongst contaminating particulates on materials surfaces exposed in space in low-Earth orbit

L. E. MURR, J. M. RIVAS, S. QUINONES, C-S. NIOU, A. H. ADVANI, B. MARQUEZ
Department of Metallurgical and Materials Engineering, The University of Texas at El Paso, El Paso, TX 79968, USA

Debris particles extracted from a small sampling region on the leading edge of the Long Duration Exposure Facility (LDEF) spacecraft have been examined by analytical transmission electron microscopy and the elemental frequency observed by energy-dispersive X-ray spectrometry and compared with upper atmosphere (Earth) particle elemental frequency and the average elemental compositions of interplanetary dust particles. A much broader elemental distribution was observed for the exposed spacecraft surface debris milieu. Numerous metal microfragment analyses, particularly aluminium and stainless steel, were compared with scanning electron microscope observations of impact crater features, and the corresponding elemental spectra on selected LDEF aluminium tray clamps and stainless steel bolts. The compositions and melt features for these impact craters and ejecta have been shown to be consistent with microcrystalline debris fragments in the case of aluminium, and these observations suggest an ever changing debris milieu on exposed surfaces for space craft and space system materials.

1. Introduction

The effects of contaminating particulates and the hazards of space and orbital debris to spacecraft and space systems and hardware have been a long-standing concern. This concern exists not only because of impact-related damage to a variety of materials surfaces and hardware functions, but also surface alterations which degrade or alter optical, electronic, thermal, and mechanical performances [1–6].

The NASA Long Duration Exposure Facility (LDEF), a 12-sided cylinder the size of a bus and weighing approximately 11 ton, was retrieved on orbit by the Shuttle *Columbia* on 12 January 1990 after it had spent approximately 5.8 years exposure of roughly 130 m^2 of surface area in low-Earth orbit (initially a nearly circular orbit of 260 miles or a final orbit of 180 miles, or 150–180 km). The 57 on-board experiments involving more than 10 000 spacecraft materials and systems test specimens were designed to allow scientists and engineers to gain a better understanding of the space environment and the effects of prolonged exposure in this environment on future space systems such as Space Station *Freedom*, and the US Strategic Defense System. Because LDEF was gravity stabilized in a non-geosynchronous orbit, each of its 26 different facing directions were constant with respect to the spacecraft's velocity vector. Upon the return and deintegration of LDEF at Kennedy Space Center, the LDEF Meteroid and Debris Special Investigation Group photo-documented data on all impacts $\geqslant 0.5$ mm for thick material surfaces and $\geqslant 0.3$ mm for thinner blanket-type materials, yielding roughly 80 impacts/m^2 on the space end and near the leading tray row. The observed ratio of leading-edge to trailing-edge impacts $\geqslant 0.5$ mm diameter was found to be 10 [7].

The Materials Special Investigation Group also found the surfaces of LDEF to be covered with a wide variety of particulate contaminants ranging in size from sub-micrometre debris to centimetre sized pieces of material; however the condition of LDEF after retrieval on orbit was not much worse than that when LDEF was launched [8]. Manufacturing, assembly, and handling residues were common. Natural airborne dusts also accumulated on LDEF surfaces. Manufacturing debris included magnetite (FeO to Fe_3O_4) spheres from welding, cutting, and grinding iron alloys, glass and carbon fibres, paint flakes, wear metals, salt spray particles, gypsum, and other minerals. Low- and high-energy micrometeorite impacts on the variety of metal, composite, polymer, and painted surfaces also created ejected particulates as well as gas phase elements. Atomic oxygen exposure generated ash and free metal foils. Paint surfaces with mineral pigments and fillers were left with free mineral particles on the surfaces and impacts redistributed these

0022–2461

materials. Glass fibre composites were often reduced to free glass fibres by atomic oxygen and silicones were oxidized to silica. In addition, a film of silicone and hydrocarbon composition estimated to weigh about 2 kg covered essentially the entire satellite surface.

Preliminary results of the chemistry of micrometeroids suggest that the analysis of projectile residues is generally very difficult partly because of the contaminated surfaces, and the fact that the structural frame and tray clamps were primarily chromic anodized 6061-T6 aluminium which often produced chromium-rich debris particles [9]. Many craters yielded no traces of projectile residues due primarily to the complete vaporization of hypervelocity impacts (> 10 km s^{-1}) [4, 10]. Chondritic compositions (calcium, silicon, magnesium and iron) [11] were observed to dominate amongst natural impact particle residues identified in craters, while other residues included man-made debris which contained titanium-, nickel- and chromium-rich compounds presumed to be related to stainless steels.

The scenario which emerges from these observations which extrapolate to nearly one billion impacts ranging down to 10 nm diameter [12] and many billions of debris particles ranging to sizes even smaller, is a dynamic, ever changing surface contamination environment complicated by cross-component contamination, orbital debris contamination, and sequential multi-impact distribution and redistribution of the surface debris milieu. While this appears at first to represent an insurmountable characterization effort, it is possible to statistically measure individual microstructures and microchemistries, and it is essential, in fact, to examine the debris milieu in order to gain a better understanding of these effects on near-term design decisions for space systems and structures development.

This paper reports some efforts to examine small particulates and debris features lifted from selected surface regions on LDEF using electron microscopy and microanalysis techniques [13, 14]. A special effort was made in this study to illustrate the relationship of micrometre-sized metal debris particles to ejecta rims and rim fragmentation especially for some of the larger micrometeoroid impacts.

2. Experimental details and analytical procedures

Miglionico *et al.* [14] have recently demonstrated the use of electron microscopy and a lift-off technique for identifying debris particles on the surface of LDEF materials. In this preliminary study not only were debris particles from other, proximate materials identified, but also particulates formed by reactions promoted by the space environment (especially atomic oxygen-induced degradation and reaction). In this study, we have utilized this modified replica technique [13] of stripping particles from the surface, and in the systematic identification of more than 100 individual particulates (mostly < 1 μm) numerous examples of aluminium and (Fe–Ni–Cr)-rich particulates were observed which were thought to arise by impact-related release of LDEF structural materials.

Approximately 75% of the exposed surface area of LDEF consisted of coated and uncoated aluminium alloys and a significant proportion of this area consisted of anodized (chromic) aluminium structural members which were held together with type 303 stainless steel bolts. All of the exposed experiment-tray flanges, nearly all the clamps, and the structural members of the LDEF frame were chromic-anodized 6061-T6 aluminium, while some Earth-end panels and a few other components were specially anodized to render them black in colour.

The experimental trays were located in bay/row locations around LDEF as illustrated in Fig. 1, which also provides the body axes definition on orbit. In the experiments to be described in this paper, standard replica-like grids (200 mesh) for transmission electron microscopy were prepared from particle regimes stripped from 6061-T6 aluminium sample surfaces [14] contained within experiment M0003 located in bay D, row 9 [7] along the leading edge of the satellite on orbit; as illustrated in the region (D09) in Fig. 1. Particles on the experimental grids were examined in an analytical transmission electron microscope (a Hitachi H-8000) operated at 200 kV accelerating potential, and fitted with a Noran energy-dispersive X-ray spectrometer for elemental analysis.

Samples of the 6061-T6 aluminium clamps and the type 303 stainless steel bolts containing large ($\geqslant 0.5$ mm) impact craters were obtained from the NASA-Johnson Space Center LDEF Curatorial Facility based upon data provided by See *et al.* [7]. Fig. 1 shows the two clamp locations designated C-1 and C-2 corresponding to deintegration numbering/

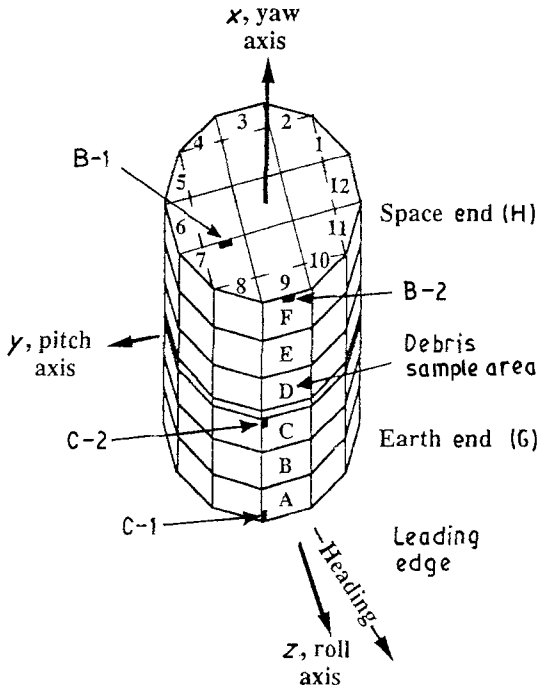

Figure 1 Schematic view showing the LDEF spacecraft body axes on orbit and the bay (A–G) and row (1–12 excluding the ends) designation. The locations of samples in this study are shown in the orientation illustrated below in Fig. 2. C-1 and C-2 indicate tray clamps while B-1 and B-2 indicate bolt locations. The diameter of LDEF was 4.6 m and its length was 92 m.

orientation schemes A09 C01 and C09 C03, respectively [7]. These samples each contained numerous impact craters with the largest measuring about 0.8 and 0.5 mm diameter for C-1 and C-2 samples, respectively.

The two bolt samples, designated B-1 and B-2 in Fig. 1, and corresponding to LDEF location numbers H07S11A and F12S04C, respectively, each contained a large impact crater measuring approximately 1.3 and 0.8 mm diameter, respectively.

Fig. 2 shows row 9 bays and other designations for orientations consistent with the schematic diagram of Fig. 1 being inspected during the deintegration process. The locations of the samples and sampled areas exposed in space (and corresponding to Fig. 1) are also designated in Fig. 2. The bolt and clamp samples illustrated in Figs 1 and 2 were cut into convenient sizes for examination in an ISI-DS130 scanning electron microscope fitted with a Princeton-Gamma Tech energy-dispersive X-ray spectrometer.

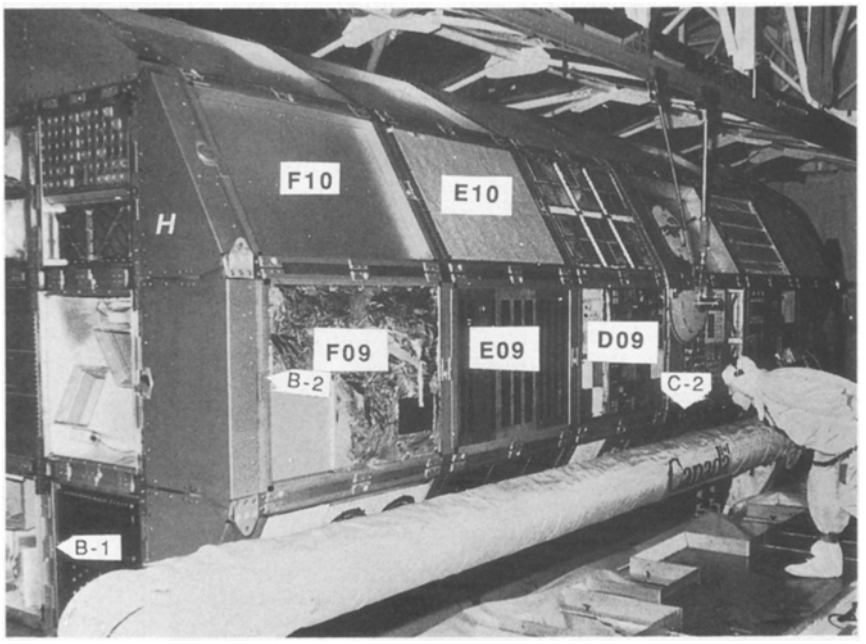

Figure 2 NASA photograph of LDEF during initial deintegration at Kennedy Space Center showing the bay/row designations illustrated schematically in Fig. 1, along with corresponding sample locations for this study. The schematic diagram in Fig. 1 must be turned 90° to coincide with the view shown in Fig. 2.

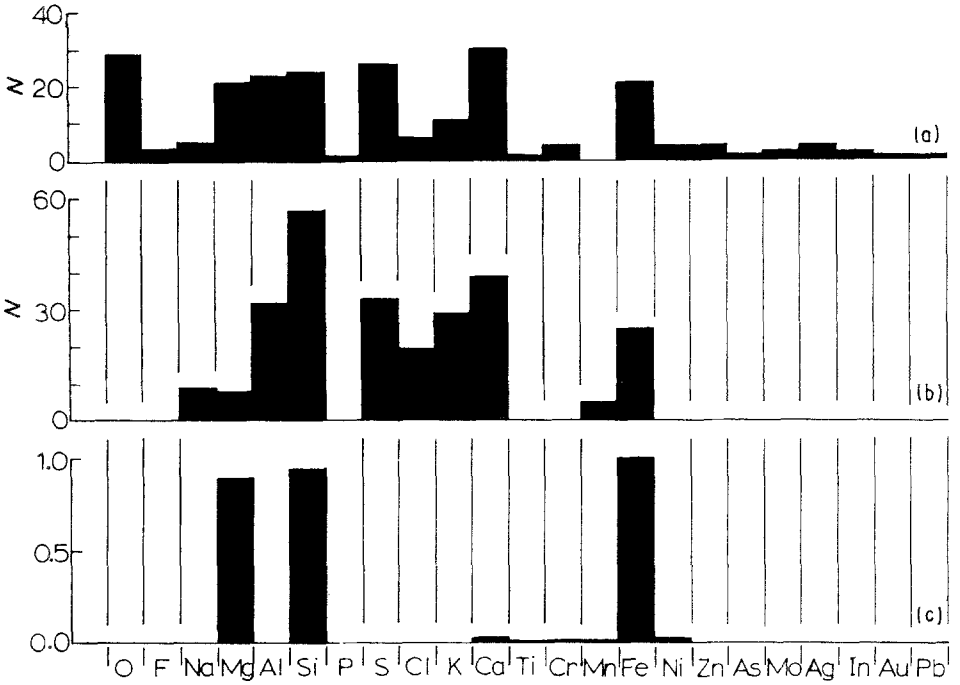

Figure 3 Comparisons of elemental frequencies or distributions in particulate regimes. (a) Experimental analysis of approximately 100 particles or debris fragments extracted from a small area in D09 from LDEF (Fig. 2): elemental frequency of occurrence is denoted by *N*. (b) Elemental analysis of more than 100 particulates in the upper atmosphere (3 km) over central New Mexico, USA, and regarded as ice-forming nuclei (IFN): elemental frequency of occurrence is denoted by *N* as in (a). (c) Elemental abundance (normalized with respect to iron) or proportion averages for chondritic micrometeoroid particles or interplanetary dust particles (IDPs) after data in [11]. This distribution contains small amounts of nickel, chromium and titanium as shown.

3. Results and observations

The examination of carbon-supported debris particulates extracted (stripped) [14] from an aluminium 6061-T6 sample surface contained within tray D09 shown in Figs 1 and 2 revealed a variety of morphologies, crystal structures, and chemistries for micrometre and submicrometre sizes which were of particular interest. Of approximately 100 individual particles or particle clusters included in this analysis several were aluminium and stainless steel compositions and other particles of apparent man-made origin such as solders, paint minerals, etc., the majority were mineral in origin (NaCl, $CaSO_4$, feldspars, etc.), and several appeared to be of space origin (chondritic: magnesium, silicon, calcium, iron) [11]. While it is difficult to compare individual particle chemistries, Fig. 3 shows for comparison the frequency of the occurrence of chemical elements in the extracted, microscopic debris particles on the LDEF aluminium alloy sample on the leading edge with a slightly larger population of ice-forming nuclei in the upper atmosphere collected over central New Mexico [15] and the elemental composition profile for chondritic interplanetary dust particles [11] plotted in the same elemental sequence. It is clear from Fig. 3 that the loadings of very small debris particles on LDEF are considerably different and more varied from Earth-upper atmosphere particles considered in the milieu of ice-forming nuclei (IFN) and the interplanetary dust particles (IDPs). A significant part of this difference, as indicated in Fig. 3, lies in the broader range of elements, particularly metals such as aluminium, iron, nickel and chromium.

Figs 4 and 5 show some examples of NaCl and $CaSO_4$ (gypsum) crystal particles typical of the debris milieu shown in Fig. 3a. These examples also illustrate

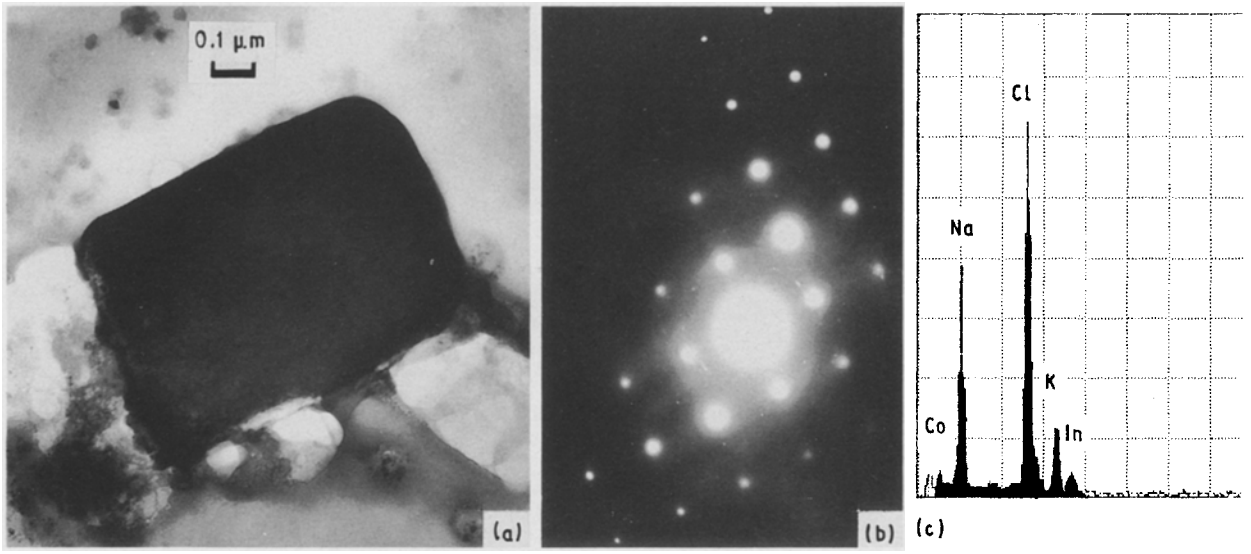

Figure 4 Typical example of salt crystal (NaCl) extracted from the LDEF sample surface. (a) TEM, bright-field image, (b) selected-area diffraction (SAD) pattern for (a), (c) EDS spectrum for (a). The particle is resting on a carbon support film.

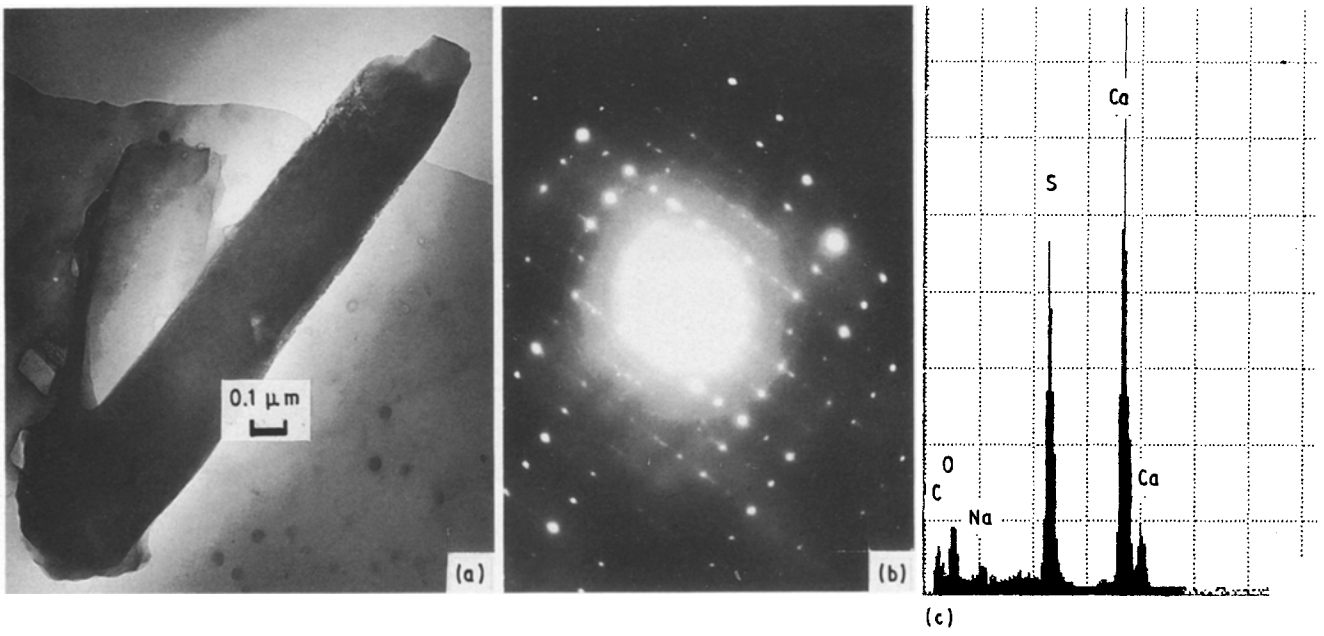

Figure 5 Typical example of gypsum crystals ($CaSO_4$) extracted from the LDEF sample surface. (a) TEM, bright-field image, (b) SAD pattern of (a), (c) EDS spectrum for (a).

the very comprehensive analysis and fine particle identification which can be achieved in the analytical transmission electron microscope. The origin of the NaCl crystals such as that shown in Fig. 4 would appear to be Earth-related rather than space-related (NaCl dendrites form on spacecraft surfaces from ejected human wastes).

The gypsum crystal, which is composed of a stack of much finer crystals as evinced in the diffraction streaks perpendicular to the crystal long axis in Fig. 5, probably originates from chalk marks found on samples in the same experiment tray in D09 (Fig. 2).

Figs 6 and 7 illustrate typical micro-debris particles characteristic of chondritic, interplanetary mineral dust (high iron content including silicon, calcium, magnesium) or geologic (mineral) origin, respectively. The interplanetary dust debris may be remnants of impact residues or fragments from impacting (impacted) particles.

Figs 8 and 9 show some examples of aluminium and stainless steel debris particles on the LDEF sample surfaces within tray area D09 (Fig. 2) which are probably impact-ejecta-related. The evidence for this origin manifests itself in the crystal structure of the fragments. Both the aluminium particle in Fig. 8 and the stainless steel fragment in Fig. 9 exhibit a very fine, polycrystalline structure, and the arrows in both Figs 8a and 9a show small diffracting grains which are as small as 0.01 μm. By contrast, these small-grain polycrystalline debris particles have their origin in impact crater ejecta which is most often melted upon impact and dynamically recrystallized during the impact and

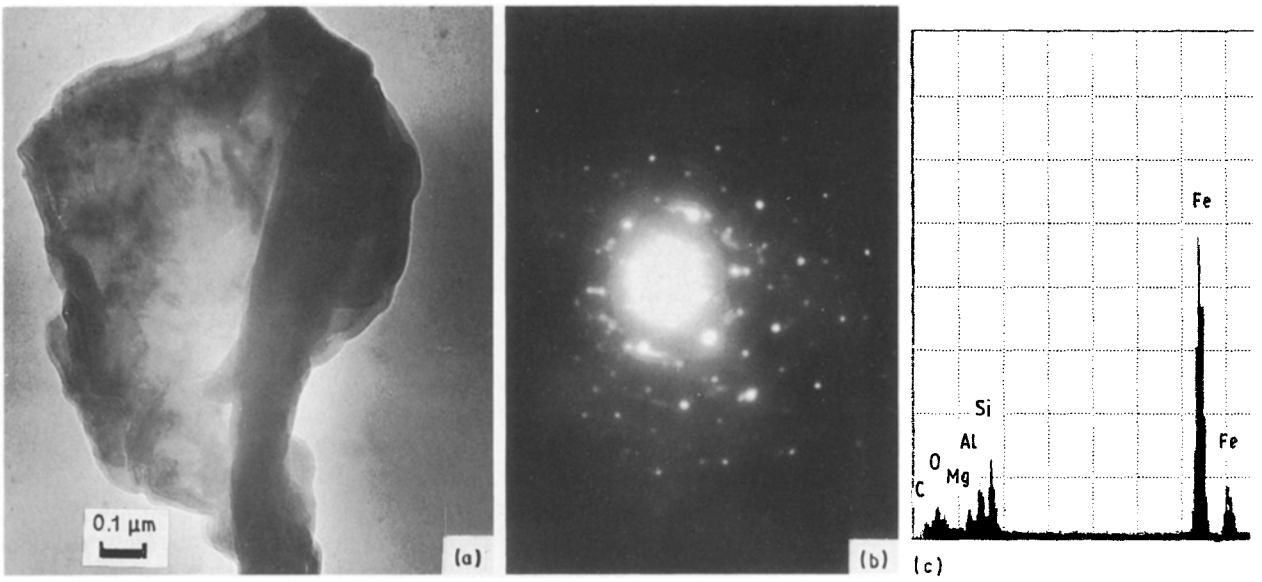

Figure 6 Chondritic (space dust)-like particle extracted from the LDEF sample surface: (a) TEM, bright-field image; (b) SAD pattern of (a); (c) EDS spectrum of (a).

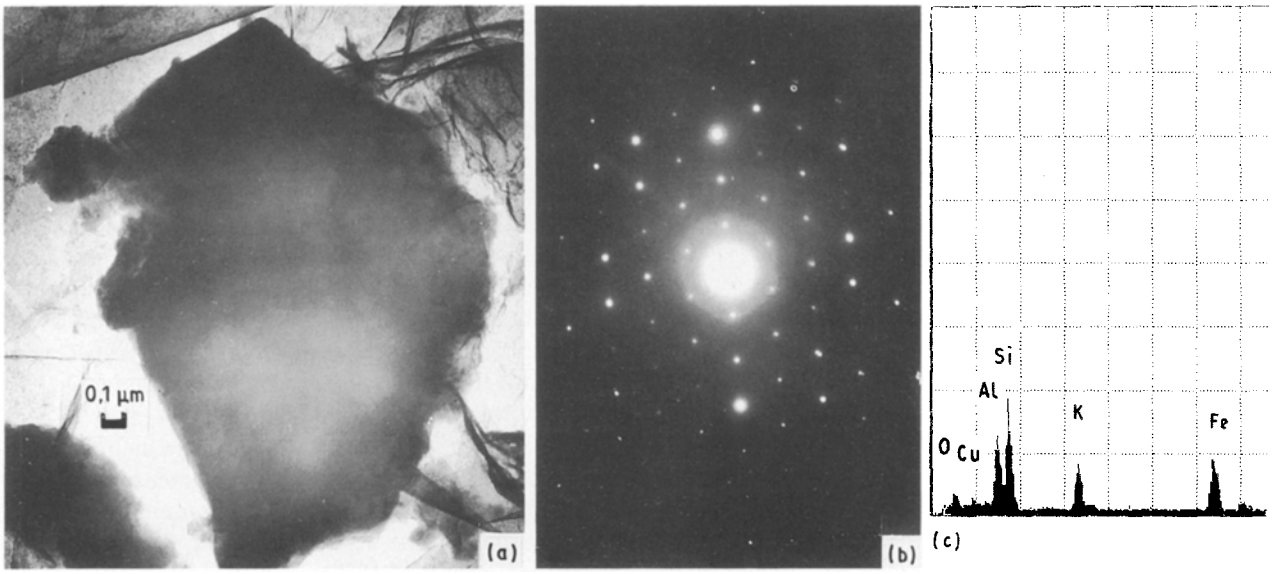

Figure 7. Mineral particle extracted from the LDEF sample surface: (a) TEM, bright-field image; (b) SAD pattern of (a); (c) EDS spectrum of (a).

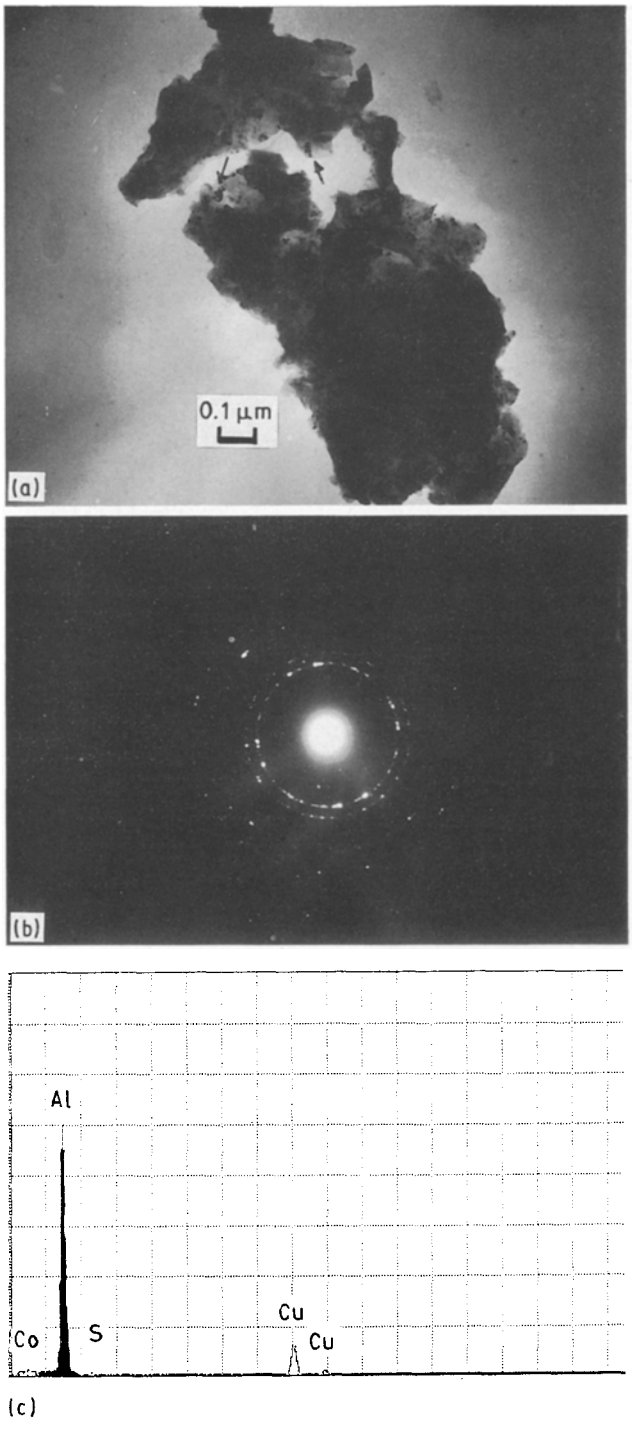

Figure 8 Aluminium debris fragment extracted from the LDEF sample surface. (a) TEM, bright-field image, (b) SAD pattern of (a), (c) EDS spectrum for (a). The copper peaks are background markers originating from the copper support grid. Arrows in (a) show small diffracting grains (or crystals).

fragmentation event, especially in the case of very high velocity (hypervelocity) impacts with commercial aluminium or stainless steel hardware components on LDEF where the as-fabricated grain sizes usually range from 50–200 μm.

While it is difficult to determine whether these debris particles came from specific material impacts, it is unlikely that those shown in Figs 8 and 9a–c came from wear fragments or microgouges of the respective surface regions, because such fragments, while often deformed, do not exhibit the extent of polycrystallinity and apparent recrystallization exhibited by the particles in Figs 8a and 9a. As a means to illustrate this, we mechanically polished (with a small size grinding powder) the surface of a type 316 stainless steel plate to create severe surface deformation. It is known that this surface deformation is most severe at the outer, ground surface and extends into the bulk a few tenths of a micrometre. To observe this feature, we used a stop-off lacquer on the deformed surface and electropolished a sample from the back side to electron transparency [13]. Fig. 9d illustrates the crystallographic nature of this surface region in contrast to that for the debris particle of Fig. 9a shown in the selected-area electron diffraction pattern of Fig. 9b. The larger reflection spots correspond to the bulk crystal structure below the deformed surface region.

While the elemental spectrum for the type 316 stainless steel shown in Fig. 9e unambiguously confirms the debris fragment in Fig. 9a to be a stainless steel, the Cr:Ni peak amplitude differences would tend to suggest that the stainless steels are indeed different as suggested. However, these ratios are often not meaningful because of the ranges of chromium and nickel content allowed in the 300 series stainless steels (16%–24% Cr and 8%–22% Ni by weight).

To examine further these assertions, we observed a range of larger impact craters ($\geqslant 0.1$ mm diameter) on aluminium (alloy) clamp and stainless steel (type 303) bolt samples from LDEF locations indicated in Figs 1 and 2. Fig. 10a shows a tilted SEM view of the largest impact crater on the aluminium clamp designated C-1 in Figs 1 and 2. The energy-dispersive X-ray spectrometer (EDS) spectrum shown in Fig. 10b contains only an aluminium peak representative of the signal from the ejecta rim region at the rear of the crater viewed in Fig. 10a. The magnified view of the crater surface looking into Fig. 10a shown in Fig. 10c clearly illustrates the residual melt-texture (including bubbles and gas escape holes) following the impact, and the view shown in Fig. 10a illustrates the fracture and fragmentation which is typical of the ejecta rims of impact craters.

Fig. 11a shows the largest impact crater on clamp sample C-2 (Figs 1 and 2) which has a smaller crater just below it. Fig. 11b shows a magnified view of the larger crater in Fig. 11a while Fig. 11c shows the EDS spectrum corresponding to the lower ejecta rim region (arrowed). It can be observed on comparing the EDS signals in Figs 10b and 11c with that shown in Fig. 8c, that the spectra are very similar.

Fig. 12a shows a low-magnification SEM view of both stainless steel bolt samples (B-1 and B-2 in Figs 1 and 2) exhibiting the largest impacts on the bolt heads. Fig. 12b shows the EDS spectrum for the bolt head near the left (and largest) impact crater. This spectrum (except for the titanium peak) is essentially identical to the microdebris fragment lifted from the LDEF sample surface as shown in Fig. 9c. The melt features of the craters and the ejecta rim fragmentation illustrated for impact craters in the aluminium clamps in Figs 10a and 11a are also prominently apparent in the magnified views of the two bolt craters shown in Fig. 12c and d, respectively. However, the titanium peak in the spectrum of Fig. 12b is vested in large

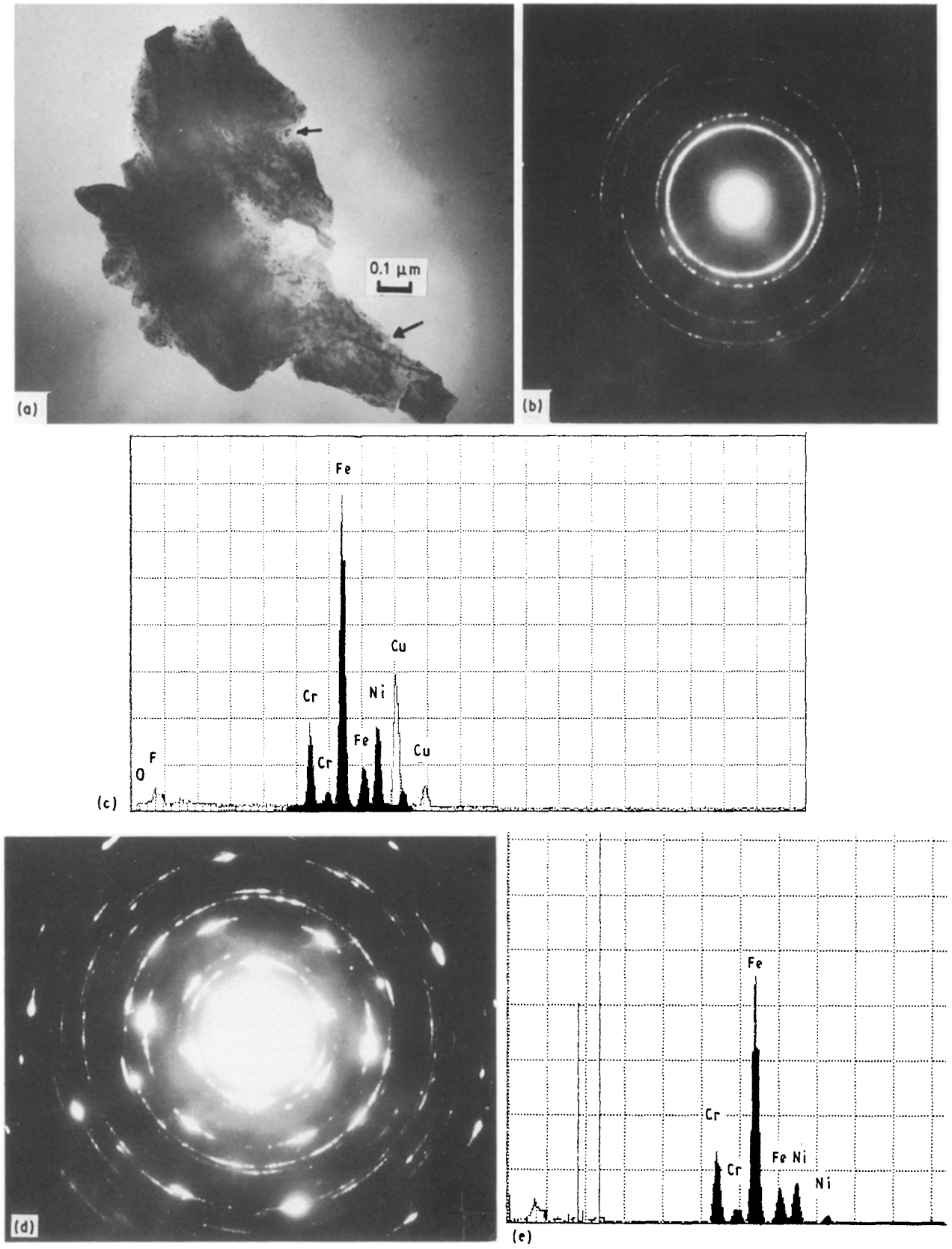

Figure 9 Stainless steel debris fragment extracted from the LDEF sample surface is shown in (a). (b, c) Corresponding SAD pattern and EDS spectrum. The copper signal arises from the copper support grid. (d) SAD pattern for thin, single-side electropolished, deformed type 316 stainless steel film. (e) EDS spectrum of (d) showing no copper peaks because the film is not supported on a copper grid. Arrows show small diffracting grains.

precipitates and this particular fragment could have originated from a bolt-related impact feature.

4. Discussion and conclusion

While the results and observations presented in Figs 3–12 are somewhat preliminary, they provide important views of the nature of the very small debris milieu which existed on LDEF, and the significant role played by microparticle impact cratering, particularly in altering the surface features, and in contributing to the debris milieu.

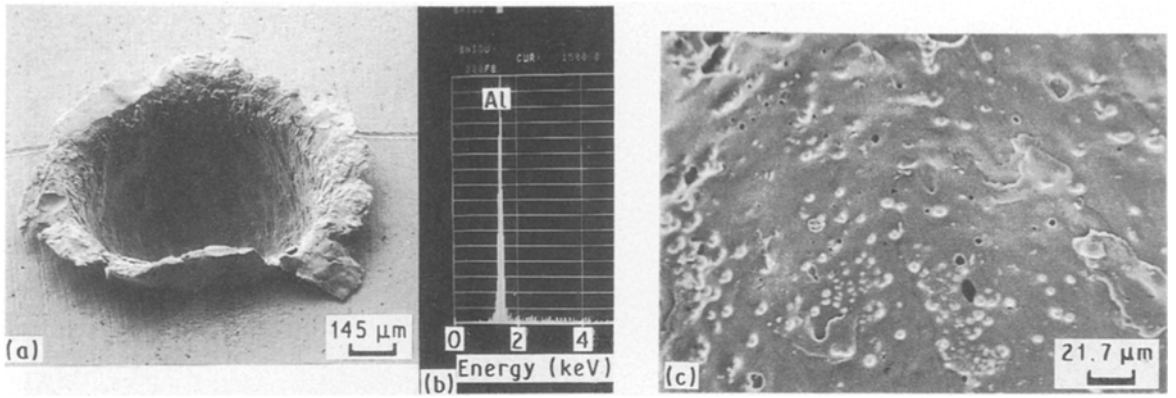

Figure 10 Impact crater in aluminium clamp (C-1) on LDEF (Fig. 2). (a) Tilted (45°) view in the SEM showing ejecta rim features. (b) EDS spectrum showing only the aluminium peak from a region inside the rear of the crater shown in (a). (c) Magnified view of crater surface in (a) showing melt features, including bubbles or blisters.

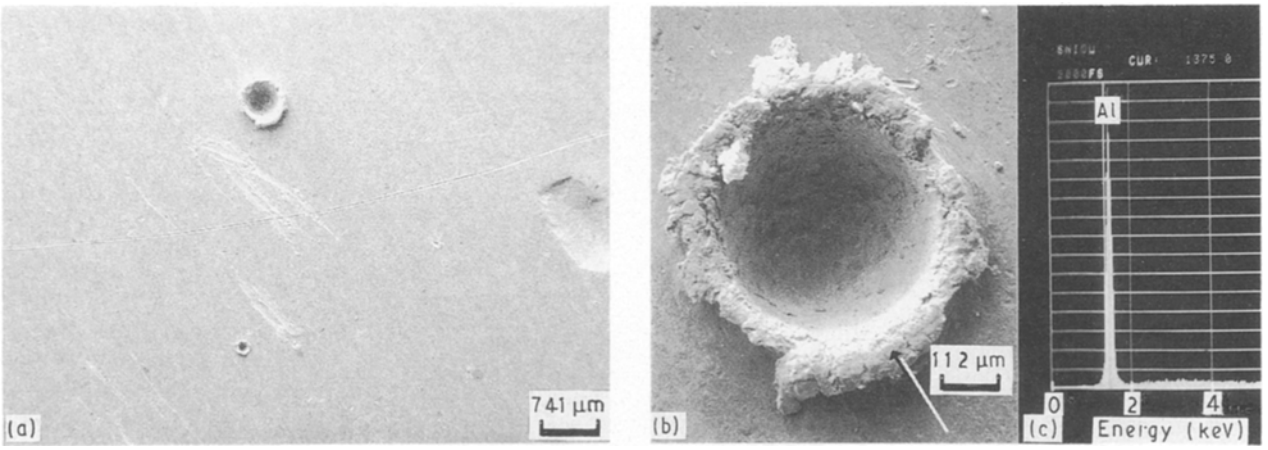

Figure 11 Impact craters in aluminium clamp (C-2) in LDEF (Fig. 2). (a) Normal SEM view showing large and smaller crater. (b) Magnified view of larger crater in (a). (c) EDS spectrum showing only aluminium peak corresponding to the ejecta rim region marked by the arrow.

Even though the cratering examples presented in Figs 10–12 were not from samples located directly within the D09 (Figs 1 and 2) tray area from which debris fragments were extracted, their analysis illustrates the strong prospects for these metal debris particles with regard to both structure of the melted and recrystallized crater rim (and ejecta fragments) and composition (as confirmed unambiguously by comparing EDS spectra). However, the NASA deintegration analysis indicated that a total of 140 impact features > 0.3 mm diameter were observed on clamps, bolts, tray flanges, and experimental surfaces in the D09 location [7]. Numerous microparticle impact craters considerably smaller than those shown in Figs 10–12 ($\leqslant 10$ μm) were, in fact, observed on the same experimental aluminium alloy surface regions from which the debris particles were extracted in the analyses presented in Figs 3a and 4–9. In addition, LDEF location E10 shown in Fig. 2 exhibited 570 impact features in the deintegration visual examination [7] which was facilitated by a uniform thermal blanket covering, with an outer (space facing) layer of FEP Teflon (~ 120 μm thick) backed by a thin silver–inconel layer. Tray F10 shown in Fig. 2 also contained the NASA Langley Research Center Space Debris Impact Experiment which consisted of aluminium 6061-T6 plates similar to those examined from D09 in this study, and contained a total of 77 impact features > 0.5 mm diameter [7].

It is clear from the comparison of particulate regimes in Fig. 3 that spacecraft surfaces will represent a very broad debris spectrum which will continually change through a variety of complex reactions and interactions, including continual impacts from space system debris, orbital debris, and space dust. However, the electron microscope, with associated spectrometric analysis capabilities, can provide a very powerful means to observe and compare the very smallest of particles in the debris milieu.

Acknowledgements

This research was supported by a NASA-Johnson Space Center Grant NAG-9-481. We are grateful for the provision of some experimental samples by C. J. Miglionico, Air Force Phillips Laboratory, and Dr Mike Zolensky, NASA–Johnson LDEF Curatorial Facility, for providing the aluminium clamp and stainless steel bolt samples from LDEF.

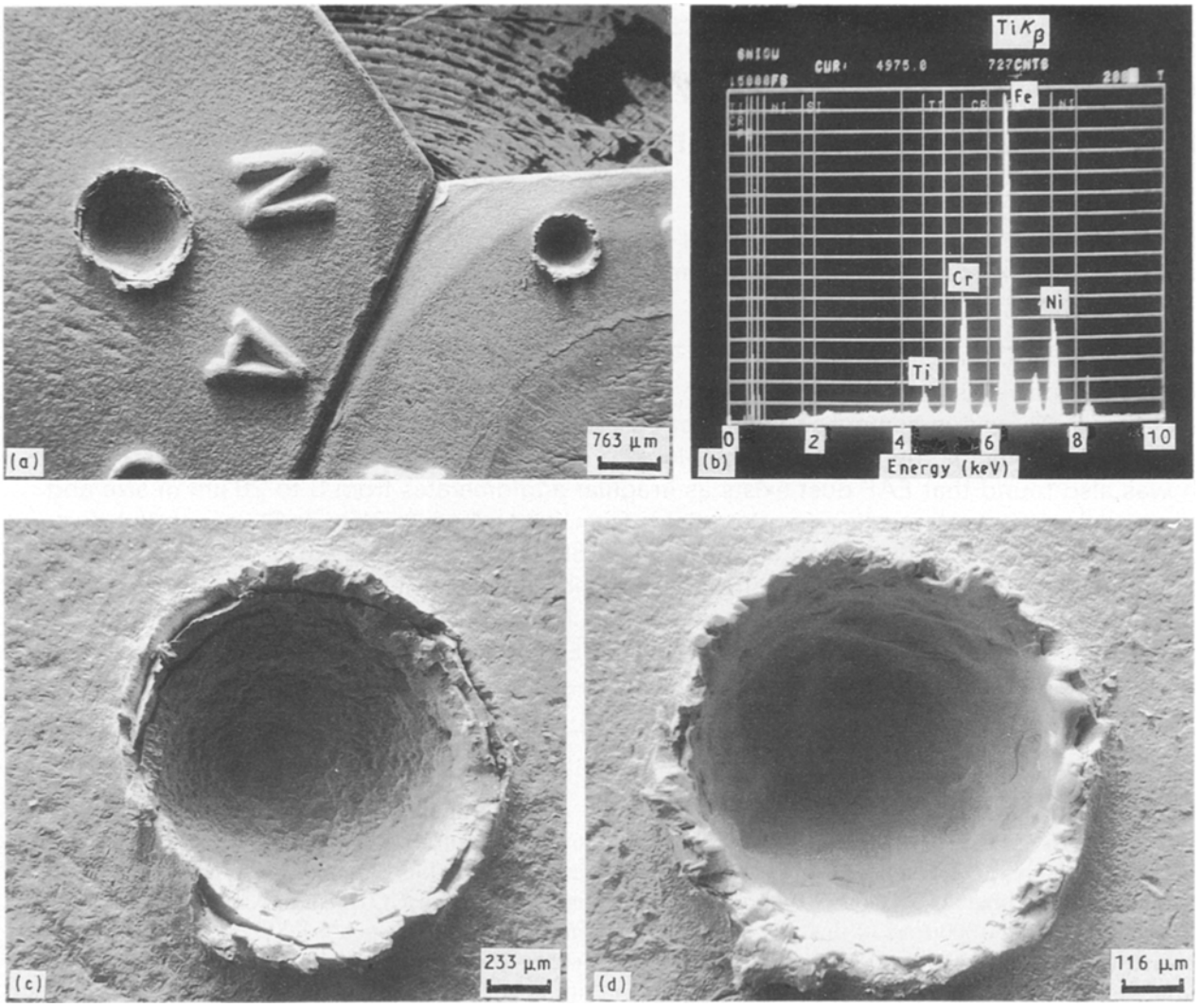

Figure 12 Impact craters in stainless steel bolts (B-1 and B-2) on LDEF (Fig. 2). (a) Low-magnification SEM view of a large crater on B-1 bolt head (left) and a smaller crater on B-2 bolt head (right). (b) EDS spectrum from a region of the left bolt surface in (a) away from the top of the crater. (c) Magnified view of the large crater in (a). (d) Magnified view of the smaller crater (right bolt head) in (a). Note melt surface features particularly prominent in (d).

References

1. E. L. WHIPPLE, in "The Physics and Medicine of the Upper Atmosphere", edited by E. L. Whipple (University of New Mexico Press, Albuquerque, NM, 1952) p. 137.
2. D. S. HALLGREN and C. L. HEMENWAY, *COSPAR Space Res.* **IX** (1969) 102
3. U. S. CLANTON, H. A. ZOOK and R. A. SCHULTZ, "Hypervelocity Impacts on the Skyles IV/Apollo Windows", in Proceedings of the 11th Lunar Planetary Science Conference, edited by G. Ryder and V. Sharpton (Lunar and Planetary Institute, Houston, TX, 1980) p. 2261.
4. B. G. COUR-PALAIS, *Int. J. Impact Eng.* **5** (1987) 221.
5. R.P. BERNHARD and D. S. McKAY, *Lunar and Planetary Science*, **XIX** (1988) 65.
6. R. UTREFA, in "Artificial Space Debris, Proceedings of Space 90 (ORBIT, 1990)", edited by N. C. Johnson and D. S. McKnight (NASA-Langley Research Center, 1990) p. 395.
7. T. SEE, M. ALLBROOKS, D. ATKINSON, C. SIMON and M. ZOLENSKY, "Micrometeroid and Debris Impact Features Documented on the Long Duration Exposure Facility: A Preliminary Report", Planetary Science Branch Publication 84 (NASA-Johnson Space Center, Houston, TX, 1990).
8. B. STEIN, "Preliminary Report on LDEF-Related Contaminants", NASA-Langley Research Center, August 1990.
9. F. HORZ, R. P. BERNHARD, T. H. SEE, J. WARREN, D-E. BROWNLEE, and M. CAURENU, in "First LDEF Post-Retrieval Symposium Abstracts", edited by A. Levine NASA Conference publication 10072 (Langley Research Center, Hampton, VA, 1991) p. 37.
10. R. KINSLOW (ed.), "High-Velocity Impact Phenomena" (Academic Press, New York, 1970).
11. D. E. BROWNLEE, D. A. TOMANDL, P. W. HODGE and F. HORZ, *Nature* **252** (1974) 667.
12. R.P. BERNHARD, private communication (1991).
13. L. E. MURR, "Electron and Ion Microscopy and Microanalysis: Principles and Applications", 2nd Ed (Marcel Dekker, New York, 1991).
14. C. J. MIGLIONICO, C. STEIN and L. E. MURR, *J. Mater. Sci.* **26** (1991) 5134.
15. J. ROSINSKI, G. MORGAN, P. WEICKMANN, J. BAIRD, A. LECINSKI, L. E. MURR and K. ERICH, *Meteorol. Rdsch.* **34** (1981) 77.

Received 27 November 1991
and accepted 18 March 1992